in **Modern Trends in Nanoscience**, eds M. Balasoiu and G. M. Arzumanyan, Romanian Academy, Bucharest, 2013, p. 29

A new approach to matter aggregation. Atomic Clusters and Nanostructures

L. C. Cune, F. D. Buzatu and M. Apostol
Department of Theoretical Physics, Institute of Atomic Physics,
Magurele-Bucharest MG-6, POBox MG-35, Romania
email: apoma@theory.nipne.ro

Abstract

The quasi-classical theoretical description of matter aggregation and solid-state cohesion at atomic level is described, in connection with its multiple applications to atomic clusters and nanostructures. The formation of isolated atomic clusters of up to 160 atoms is presented and characterized with respect to geometric forms, atomic positions, inter-atomic distances, ground-states and isomers, binding energies, magic numbers, vibration spectra, and the derivation of single-particle properties is outlined, within the point-like ions approximation. The surface of a semi-infinite solid is characterized within the same approach, and the formation of clusters deposited on surfaces is described, with regard to similar physical and chemical information. Peculiar nanostructures are also presented, as resulting from computation process, as an indication of the large variety of possible nanostructured forms. The extension of the theoretical tools to more complex situations, in particular to directional bonds and quantum corrections, is also discussed. More general effective inter-atomic potentials are given, as resulting from the present quasi-classical description.

1 Introduction

The great deal of activity and interest recorded at present in nanoscience and nanotechnologies raises basic issues of matter aggregation and structuration at the atomic level. While enabling major breakthroughs in life sciences and medicine, ultraminiatural electronics, materials, tools and processes, and manipulating individual atoms at the same time, the nanoscale

sciences provide a more direct, sensible representation of the atomic and molecular matter, together with a more accurate knowledge of the physical and chemical structures and processes at this level. Traditionally, the field bears relevance upon chemical bonding of molecules and solid-state bulk bodies. However, in-between there is an extremely large amount of various kinds of supramolecules, molecular aggregates, atomic clusters, nanostructures and nano-objects, either isolated or in various environments, sometime exhibiting intricate geometries and beautiful symmetries, with their own specific behaviour. This immense new realm that fills plenty in the "room at the bottom", according to a famous Feynman's statement, displays basically a quantum behaviour and a size dependence. These issues are addressed in the present paper, from the perspective of the quasi-classical description of ensembles of valence electrons and charge-compensating point-like ionic cores, with particular emphasis on relevant physical and chemical information on various atomic clusters and nanostructures, both isolated or under various geometric constraints as, for instance, clusters deposited on surfaces. In particular, geometric forms, atomic positions, inter-atomic distances, binding energies, magic numbers and vibration spectra are presented, and the extension to single-particle properties and structured ionic cores is outlined. Within given approximation, the results are applicable to homo-atomic metallic formations. The results described here are based on an original theory of the authors, which shows that matter aggregation follows from the delocalization of the electronic wavefunctions, the quantum statistics of the fermions (Pauli exclusion principle) and the Coulomb interaction.

2 Theory

In chemical binding the single-electron wavefunctions are superpositions of localized atomic-like orbitals and extended bond-like orbitals. Due to the great disparity in the spatial scales of the two types of orbitals the problem of the nuclei-electrons interaction is separated into a purely atomic-like part, a chemical-bond part, and a residual interaction which can further be removed by using classical variational principles.[1] The atomic-like part can be treated by standard ab-initio wavefunctions method,[2] while for the chemical-bond part a quasi-classical description has been developed recently,[3] in close connection with the density-functional method.[4] For the chemical-bond part we are left with an ensemble of electrons moving in a background of neutralizing effective charges in the valence upper shells of the ions. These charges are distributed in space according to the corresponding atomic-like orbitals,

but we adopt here, for the sake of the simplicity, a point-like distribution

$$\rho(\mathbf{r}) = \sum_{i=1}^{N} z_i^* \delta(\mathbf{r} - \mathbf{R}_i) \ , \tag{1}$$

where z_i^* are the effective charges (in units of electron charge e) and $\mathbf{R}_i$ denote the positions of N ions, $i = 1, 2, ...N$. Such a point-like ionic charge distribution bears a limited relevance upon certain s-, d- and f-metallic ions, where we may neglect the radial dependence of the atomic-like orbitals and average out their angular dependence, but it is inadequate for an important, very large class of ions with p-valence orbitals, or with hybridized valence orbitals. The effective charges can, in principle, be obtained by solving the entire problem of nuclei-electrons interaction, as remarked above, but results are not yet available. However, for certain ions, within the point-like approximation, we may estimate the effective charges by making use of the atomic screening theory.[5] For instance, we get $z^* = 0.57$ for Fe^{2+}(iron), $z^* = 0.34$ for Ba^{2+}(barium), and $z^* = 0.44$ for Na^{1+} (sodium). Such estimations, together with the point-like approximation, render a status of model-calculations to the results presented herein. In addition, the theoretical treatment employed here is valid for a sufficiently large number N of not-too-light atoms.

Within the quasi-classical description of the Hartree-Fock equations[3] the chemical-bond orbitals are quasi-plane waves in the first approximation, and the electrons move in the Hartree self-consistent field

$$\varphi(\mathbf{r}) = \sum_{i=1}^{N} \frac{z_i^*}{|\mathbf{r} - \mathbf{R}_i|} e^{-q|\mathbf{r}-\mathbf{R}_i|} \tag{2}$$

corresponding to the charge distribution given by (1), where q is a screening wavevector similar to the Thomas-Fermi wavevector, to be determined variationally. The self-consistency requires a linear relationship $n = (q^2/4\pi)\varphi$ between the electron density n and the potential φ, which allows a straightforward computation of the interaction energy. This energy includes the Coulomb attraction betwen electrons and ions and the Coulomb repulsions both between electrons and between ions, respectively; we call it potential energy, and it is given by

$$E_{pot} = -\frac{3}{4} q \sum_{i=1}^{N} z_i^{*2} + \frac{1}{2} \sum_{i \neq j=1}^{N} \Phi(R_{ij}) \ , \tag{3}$$

where

$$\Phi(R_{ij}) = -\frac{1}{2} q z_i^* z_j^* (1 - \frac{2}{qR_{ij}}) e^{-qR_{ij}} \tag{4}$$

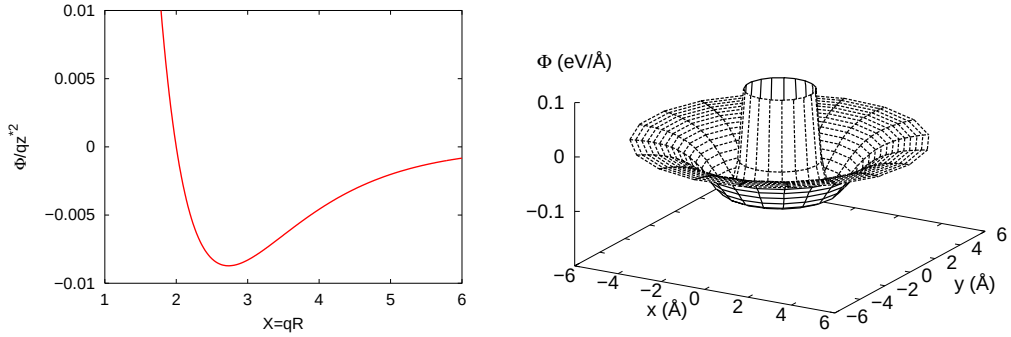

(a) (b)

Figure 1: (a) The inter-ionic potential function *vs* reduced distance. (b) A two-dimensional sheet of the inter-ionic potential (4) for Fe-ions.

is the effective (pseudo-) potential acting between two ions separated by the distance $R_{ij} = |\mathbf{R}_i - \mathbf{R}_j|$. This inter-ionic potential is shown in Fig. 1. It has an attractive tail at long distances and is strongly repulsive at short distances.

We emphasize that the inter-atomic potential given by equation (4) is derived from rigurous theoretical principles and is a new potential, in comparison with many quasi-empirical potentials used to simulate the matter aggregation. This potential has beed discovered in 2000 by one of the co-auhors of the present paper (L. C. Cune). The interacting part in E_{pot} is the only contribution which depends on the ionic positions, so that we may minimize this energy represented by the second term in the *r.h.s.* of (3) with respect to $\mathbf{R}_i$ (actually with respect to the dimensionless variables $\mathbf{X}_i = q\mathbf{R}_i$) in order to get the equilibrium forms of the ensemble of ions; doing so, we get both the ground-state of the ionic aggregate and the isomers, which differ by slight changes in energy and ionic positions. They correspond to local minima of the potential energy (3). The minimum values of the interacting part in (3) is usually very small in comparison with the self-energy ionic part given by the first term in the *r.h.s.* of (3), so we may neglect this contribution in approximate estimations. The model of metal obtained here resembles very much the old Wigner-Seitz model.[6]

The quasi-classical description is based upon slight spatial variations of the electron density in extended chemical-bonds orbitals; this enables the linear self-consistency relationship given above between electron density and potential. Accordingly, such a linearization is in order for the kinetic energy of the electrons too; it reads[1] $E_{kin} = (27\pi^2/640)q^4 \sum_i z_i^*$. The quasi-classical

[1]In atomic units $e^2/a_H \cong 27.2$eV, where $a_H = \hbar^2/me^2 \cong 0.53$Åis the Bohr radius ($m$

energy $E_q = E_{kin} + E_{pot}$ is then obtained, where E_{pot} is the ground-state minimum value of the potential energy (3), and minimized with respect to the screening wavevector q. It is easy to see that such a minimum value exists; for homo-atomic aggregates it is given by $q \simeq 0.77 z^{*1/3}$, neglecting the small contribution of the interacting part to the potential energy at equilibrium. In this case we may also define an average inter-ionic distance a by $aq \simeq 2.73$, where $X = 2.73$ is the reduced distance; for this distance the inter-ionic potential (4) reaches its minimum value.

The exchange energy in the Hartree-Fock equations admits plane waves as eigenstates. More, it remains unchanged for quasi-plane waves, *i.e.* for slight local changes in the electron density, as in the quasi-classical description, due to its non-local character;[2] it follows that screening does not affect it in this approximation, so we may simply add its (linearized) contribution $E_{ex} = -(9/32)q^2 \sum_i z_i^*$ to the quasi-classical energy E_q, with q determined above, to obtain the binding energy $E = E_q + E_{ex}$. For homo-atomic aggregates the ground-state energy is given by $E = -N(0.43 z^{*7/3} + 0.17 z^{*5/3})$, leaving aside the small contribution of the interacting part of (3) (which however is responsible for the non-thermodynamic behaviour and the size dependence).

The theoretical scheme outlined above is a linearized Thomas-Fermi model in fact, as derived from the quasi-classical solution of the Hartree-Fock equations. It differs from the standard non-linear Thomas-Fermi model (characterized by $n \sim \varphi^{3/2}$) in that it exhibits binding of the interacting ions and electrons, in contrast to the latter where there is no binding.[8] The non-linear Thomas-Fermi model is valid in the limit of infinite ionic charges (so-called quasi-classical limit), while the linearized model presented here is the starting point of the quantum behaviour of matter aggregation, and it could represent the solution to chemical bonding Schwinger was alluding to.[9] It has been applied to heavy atoms (with atomic numbers $Z \gg 1$) where the well-known binding energy $-16 Z^{7/3}$eV has been successfully reproduced (quantum corrections included), to a consistent analysis of bulk properties of a model of "universal" metal, and to realistic estimations of the ionization potentials of metallic clusters.[10] The quasi-classical description as presented above is only the first step in a full treatment. It offers the great advantage of getting structured atomic ensembles with rather limited computational resources. On the other hand, it offers the possibility of pursuing consistently the so-called quantum corrections. The latter include the ab-initio computation of the effective charge parameters as indicated before, taking into account the

is the electron mass and $\hbar$ denotes the Planck constant).

[2] This "rigidity" character of the exchange energy has been noticed probably for the first time by Slater;[7] see also Ref. 6.

entire problem of nuclei-electrons interaction, as well as the single-particle properties, in particular the single-electron energy levels of the electrons motion in the self-consistent potential φ, as given by (2), for instance.[3] These corrections bring certain changes in energies and, consequently, equilibrium ionic positions, as well as other relevant quantities. The quantum corrections are basically due to the strong variations of the electron density and self-consistent potential over small distances of the order of atomic distances. These deviations can be estimated, if one considers, for instance, the screening wavevector q as related to the average of the Fermi wavevector; doing so, we obtain $\sim 17\%$ an accuracy of the quasi-classical results. Further on, the single-particle wavefunctions of the Hartree-Fock equations entail an inherent second-order uncertainty in the self-consistency scheme, which signals its limits; therefore, we conclude that, once the quantum corrections included, the results are valid within at most $\sim 0.17 \times 17\% \simeq 3\%$ accuracy, and this would be the limit of the approach.

3 Metallic Clusters

The first step in applying the method described above is to minimize the potential energy given by (3) and (4) with respect to the reduced ionic positions $\mathbf{X}_i = q\mathbf{R}_i$. Since the $\mathbf{X}$-dependence of the potential function Φ does not involve the nature of the ions, the equilibrium geometric forms found by such a minimization are universal. The minimization method is implemented by giving originally ionic positions randomly distributed in space, computing the forces at each position, and letting the ions move step by step in the direction of the forces, until an equilibrium is reached (actually until the forces are less than 10^{-4}eV/Å).

The equilibrium positions can correspond either to the ground-state or to isomers. In order to distinguish the ground-state from the isomers we run several hundreds times the equilibrium process for each atomic aggregate, attempting to get a statistical ensemble as large as possible. In addition, for differentiating between local minima and saddle-points we compute also the vibration spectra in the harmonic-oscillator approximation. Finally, we compute the quasi-classical energy E_q, find out its minimum value and the screening wavevector q, add the exchange energy E_{ex} and get the binding energy E for the ground-state, as described in Section 2. The latter exhibits small, irregular variations with respect to the number N of atoms; to put them clearly into evidence we compute also the so-called abundance, or mass spectrum, as given by $D = \ln(I_N^2/I_{N+1}I_{N-1}) = E(N+1)+E(N-1)-2E(N)$,

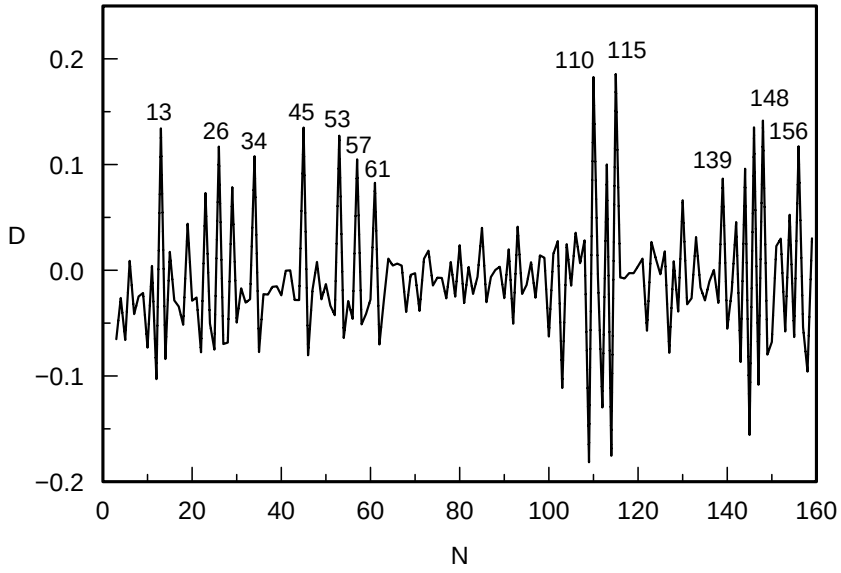

Figure 2: Ground-state mass spectrum of metallic clusters.

where I_N is the Boltzmann statistical weight for the ground-state. It is found that such a spectrum does not depend on the effective charges z^* within reasonably large limits. This procedure has been applied to homo-atomic clusters of metallic ions up to $N = 160$.

The mass spectrum of homo-atomic metallic clusters is shown in Fig. 2. It exhibits a sequence of high and very sharp peaks, corresponding to what we call magic clusters. Indeed, these magic clusters in their ground-states are much more stable as compared to their neighbours, and may possess a high symmetry, most of them a pentagonal one, like the centered icosahedron $N = 13$. Some of these magic clusters are shown in Fig. 3. For relatively small values of N we expect to get Plato's perfect polihedra; however, this is not always true; for instance, we obtain the tetrahedron ($N = 4$) and the octahedron ($N = 6$), but the hexahedron (cube, $N = 8$) and the dodecahedron ($N = 20$) are not ground-states (we get them as isomers), while the icosahedron prefers to be centered ($N = 13$). It seems that the principle of atomic packing in such magic clusters is a certain "space economy". Indeed, this can be shown convincingly on the three "most magic" clusters shown in Fig. 4, with $N = 45, 110$ and 115, respectively. The first row in Fig. 4 shows a front view which displays the highly symmetric forms of these clusters, while their outer shells are shown in the second row; indeed, such clusters are made of multiple, closed geometric atomic shells, with one shell's atoms placed just above the facets' centers of another. These

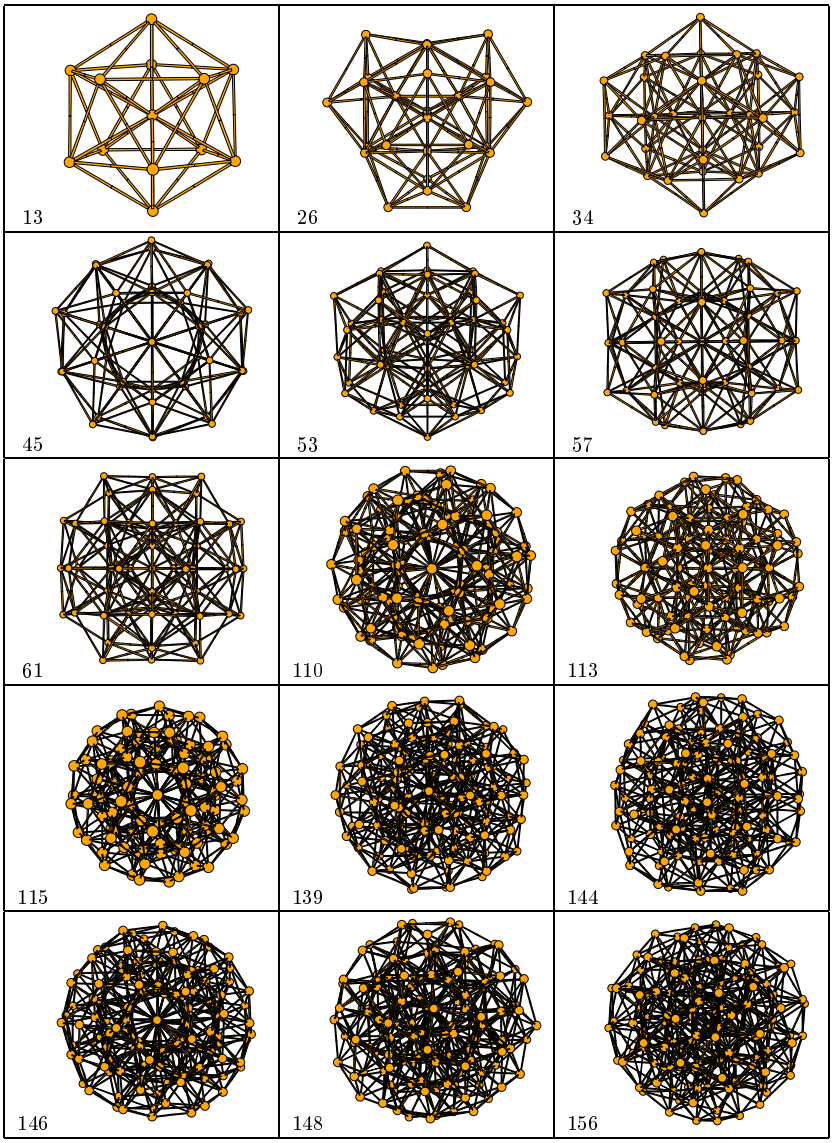

Figure 3: Magic clusters of metallic ions.

clusters display an outstanding five-fold symmetry, yet other magic clusters, though very close to a high symmetry, exhibits also slight, disconcerting imperfections, like the $N = 113, 144$, or 148 clusters in Fig. 3. It is worth noting here that some of these structures have also been obtained either by other theoretical techniques, or have been identified experimentally,[11] and the five-fold symmetry magic numbers like $N = 13, 45, 115$ are known as geometric, or icosahedral magic numbers. As regards a possible comparison with experimental results a word of caution is in order here. First, it

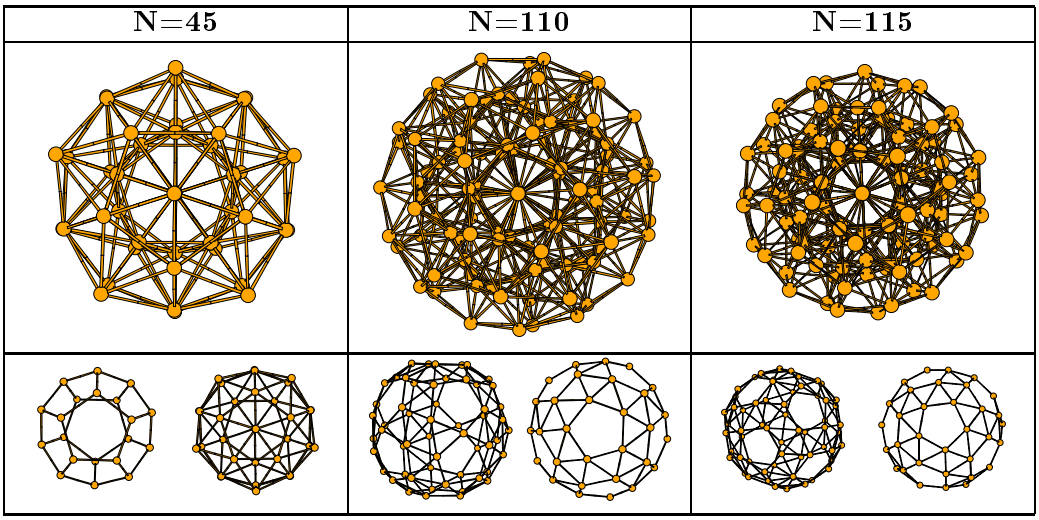

Figure 4: Highly-symmetric metallic clusers (first row), displaying outer shells (second row).

must be stressed that the mass spectrum given in Fig. 2 corresponds to the ground-states, while clusters are usually produced experimentally in a statistical ensemble at a non-vanishing temperature. Consequently, a statistical average is relevant for experimental abundance, which includes isomers beside the ground-state; this gives "statistical" magic numbers N, as distinct from the present "geometric", or "ground-state" magic numbers given in Fig. 2. A table of isomers is given in Fig. 5 for Fe-clusters, where we may notice an increase in the number of isomers on increasing size, as well as several "white islands" placed approximately at the magic clusters (for instance at $N = 13$, 45 and 115), as expected. Similarly, it is worth noting that slight differences in energy differentiate the isomers from the ground-states. Secondly, "electronic" magic numbers may be obtained, as different from the two previous ones, from the filling up of the electron states in model potentials, like the well-known quadropole-deformed harmonic-oscillator potential. In particular, the latter potential is obtained from the self-consistent potential (2) in the long-wavelengths (continuum) limit,[3] which may be relevant for other sets of experimental data, depending on the clusters nature and the particular conditions of producing these clusters.

Having obtained the equilibrium ionic coordinates $\mathbf{X}_i$ by minimization of the potential energy, and the screening wavevector q from the minimum value of the quasi-classical energy, we may obtain the inter-ionic distances $R_{ij} = X_{ij}/q$ at equilibrium; on the average they are of the order of $2-3$Å. It is worth noting that for computing such quantities, as well as for computing

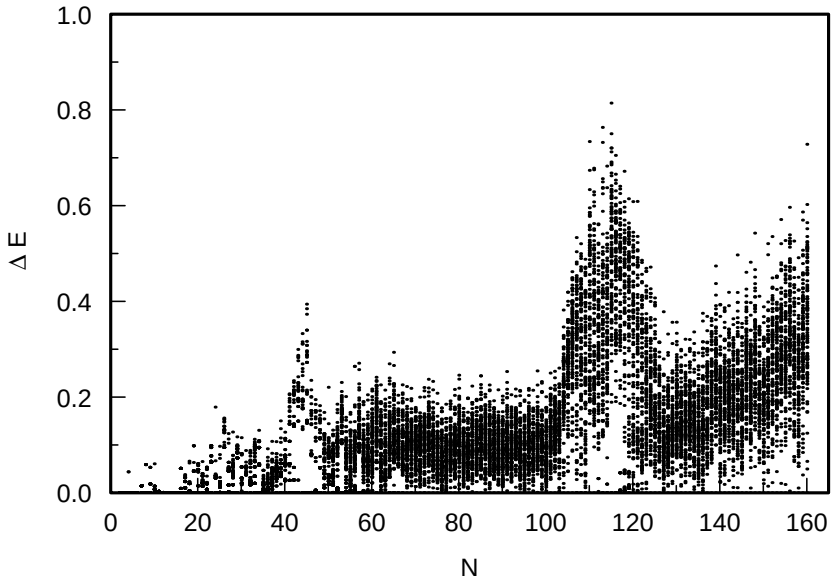

Figure 5: Isomer table of Fe-clusters.

the binding energy or the vibration spectra, one needs to know the nature of the atomic species, in particular the effective charges z^*. The vibration spectra for several magic clusters of Fe in the ground state are shown in Fig. 6. One can notice the increase of low-energy vibration states density with increasing cluster size, as expected, as well as higher multiplicity of the vibrational states for more symmetric clusters. The binding energy per atom for the ground state of Fe-clusters ($z^* = 0.57$) is given in Fig. 7 *vs* cluster size N. The binding energies of such clusters are of the order of $5 - 6$ eV per atom. These numerical values are in good agreement with the results of other computations.[12] In this respect, it is worth mentioning the large amount of work devoted to metallic clusters, by employing both ab-initio calculations, molecular dynamics, density functionals, or jellium-like models; numerical data, when available, can be found, for instance, in Ref. 13.

The results presented here suggest that metallic clusters produced experimentally by various techniques may have very likely equilibrium geometric forms like those given in Fig. 3 for their ground-states, or slightly different ones for their isomers. Most metallic clusters serve as cores for more complex, nanostructured aggregates, like organo-metallic clusters (as we shall see in the next section), and the core geometry brings useful information in designing the structure and the functionality of the latter. The presence of the isomers, which are separated from the ground-state by small amounts of energy, is particularly interesting in giving indication about cluster stabil-

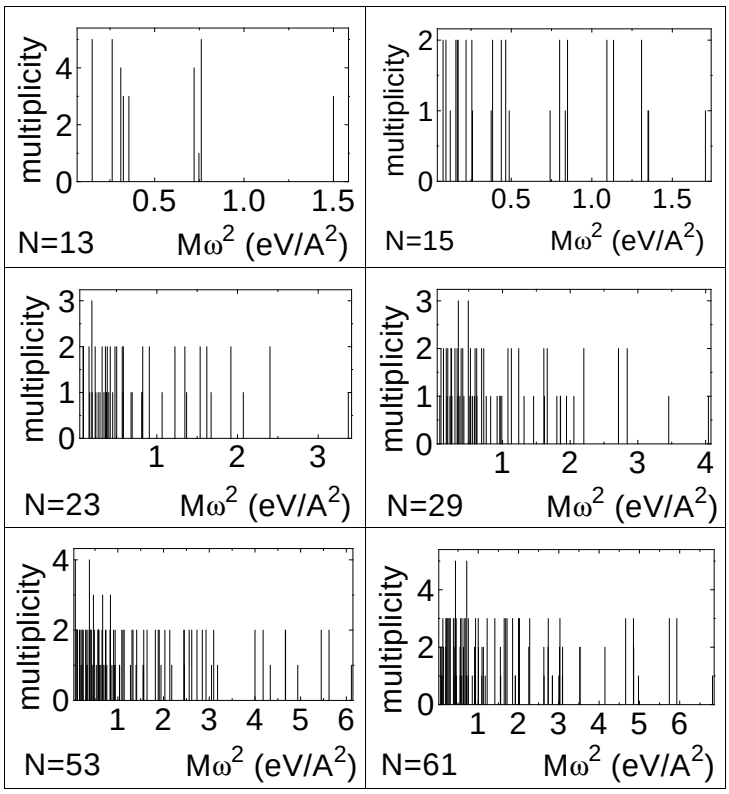

Figure 6: Ground-state vibration spectra of ground-state Fe-clusters.

ity and their possible tunneling between various geometric configurations; a privileged position in this connection have the magic clusters associated with "white islands" in the isomer table in Fig. 5, but the origin of the rather wide energy gaps between the ground-state and the first excited state in this case is not known; at most, we can trace it back to a rather vague principle of "space economy", as said above.

4 Particular Nanostructures

The theoretical model of atomic aggregation presented in Section 2 can also be applied to more complex clusters. Such a complex organo-metallic cluster is the iron-hydrocarbonated $Fe_{13}(C_2H_2)_6$ which has recently been synthesized experimentally.[14] Since each CH-radical may bind to a Fe-ion by taking one valence electron, it seems naturally to assume that 12 Fe-ions possess half of the effective charge of a standard Fe-ion, *i.e.* $z^* = 0.57/2 = 0.28$, and view the entire structure as consisting of 12 such Fe-CH ions and one

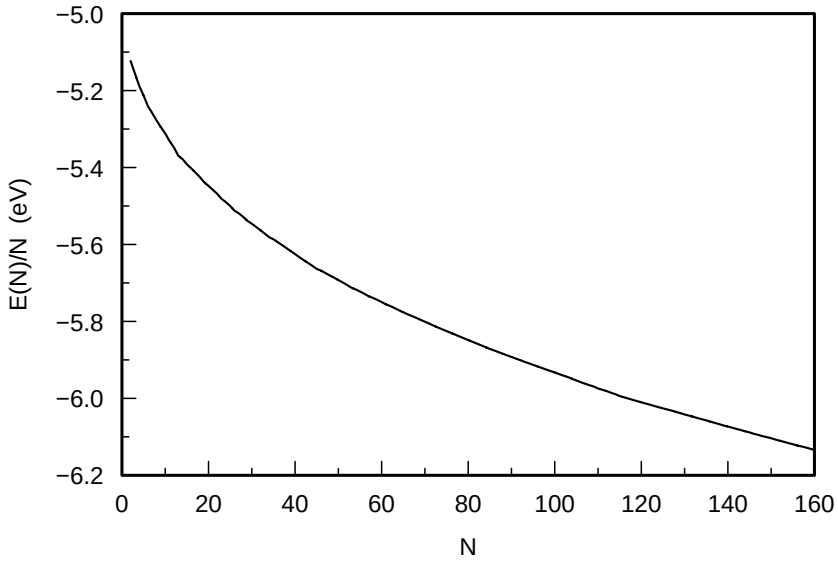

Figure 7: Ground-state energy per atom of Fe-clusters *vs* cluster size.

standard Fe-ion (with effective charge $z^* = 0.57$). Such a structure clusterizes into a centered perfect icosahedron as the one shown in Fig. 3 for $N = 13$, which may be viewed as the core of the actual organo-metallic cluster $Fe_{13}(C_2H_2)_6$. Simple arguments of a minimal interaction energy between the C_2H_2-acetylene radicals lead then to a symmetric arrangement of them on the surface of the Fe-core cluster, as shown in Fig. 8. The contribution of the metallic core to the binding energy has been estimated, as well as the inter-atomic distances, vibration spectrum and the electron charge distribution,[15] getting thus useful preliminary information for a more detailed study, which must include the directional bonding of the C_2H_2- radicals.

A more complex experiment has been run on computer by making use of the present theory. It consists of giving 8^3-unit cells of a *bcc*-metal and let the ions relax to equilibrium. Doing so, a huge cluster of $N = 855$ atoms has been obtained as shown in Fig. 9a, with a pretty disordered structure, which however preserves an approximate original *bcc*-symmetry in a core of about 3 unit cells, as shown in Fig. 9b. The computations take a rather long time in this case, and the statistics of the results is poor enough to have a reliable structure. However, this may give useful indications as to how the translation symmetry of a bulk solid may appear on increasing the number of atoms, and the extent of the surface (finite-size) effects. It has also found that the isomers of such a chunk of solid are extremely numerous, within a narrow energy range just above the ground-state energy, as expected, but, what is very interesting, they are associated mainly with slight, multiple changes in

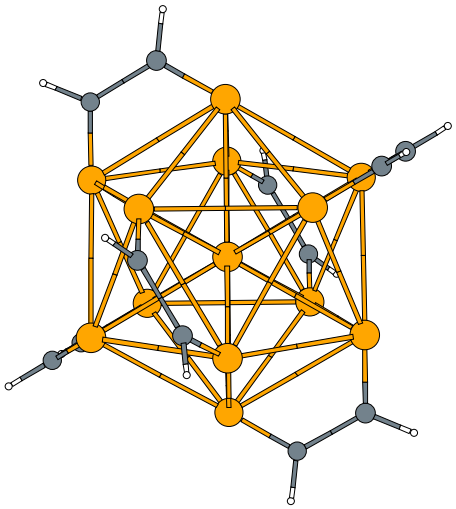

Figure 8: A $Fe_{13}(C_2H_2)_6$ cluster (Refs. 14, 15).

the positions of the outer ions. It suggests that the surface of a very large cluster, or of a solid, might be fuzzy, as corresponding to a superposition of states with slightly different atomic positions, very similar to a liquid (it may be termed a "quasi-liquid"). Such a picture may have important significance for friction.

In some computer runnings various peculiar nanostructures have been obtained accidentally, each with suggestive particularities. For instance, we got an atomic sheet with an almost perfect hexagonal symmetry, as shown in Fig. 10a, which is unstable, as expected (it may be stabilized by depositing it on

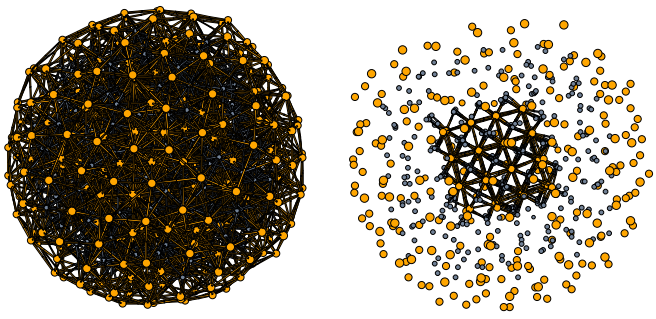

(a) (b)

Figure 9: (a) An 855-atoms bit of metal. (b) A *bcc*-core of an 855-atoms metal.

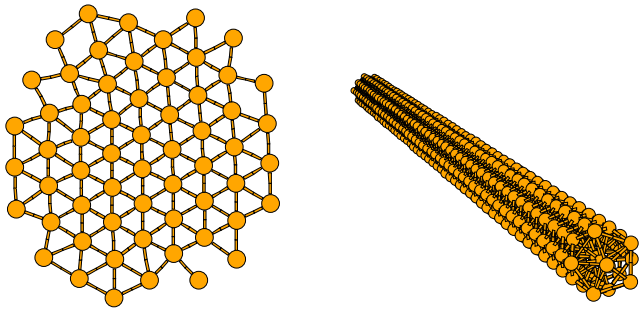

(a) (b)

Figure 10: (a) An unstable hexagonal metallic sheet. (b) A metallic popcorn wire (unstable).

a surface); or unstable chains of metallic ions, the most interesting being the one shown in Fig. 10b; it consists of a sequence of intertwined, mutually rotated icosahedra, leaving outside one protruding icosahedral end-atom, which might be suggestive for a perfect probe tip in scanning microscopy. The chain is however unstable, as expected for such a simplified one-dimensional model of metal, but its diameter is smaller than the inner diameter of a carbon nanotube, so the latter may act as a stabilizing support. The results obtained within the present theoretical approach for such low-dimensional nanostructures, beside their suggestive character, may be useful as a constitutive input for more elaborate theoretical models.

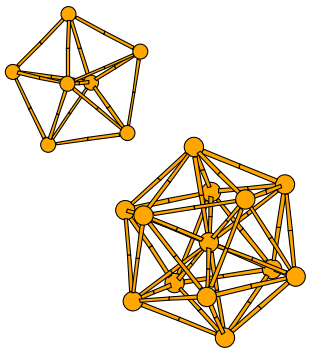

Figure 11: Two weakly interacting metallic clusters.

Another very interesting situations appeared in a few computer runnings where a number of metallic ions aggregated spontaneously in a two-clusters structure as shown in Fig. 11; the two aggregates interact extremely weakly, and end by forming one connected cluster after a very long while. The

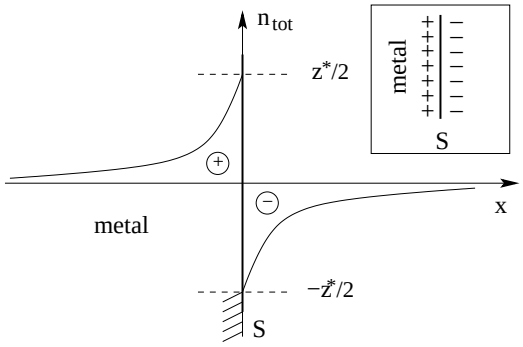

Figure 12: Charge distribution at the metallic surface double layer.

occurrence of such disconnected atomic structures originates in the separable nature of the interaction (3) with respect to the ionic positions.

Some of the peculiar nanostructures described above may be stabilized either by geometric constraints (as, for instance, depositing them on surfaces, as we shall see in the next section), or by dynamic constraints. Indeed, we may apply a tension for instance on the two end-atoms of, say, the perfect 13-atoms icosahedron (or more complex structures), as produced by two forces acting in opposite directions, and look for equilibrium forms of such a distorted cluster. It is found that there are several discrete equilibrium forms until the breaking of the cluster, and the transverse size of the cluster is successively diminished in steps on increasing the applied force. These steps are very close to "atomic steps", corresponding to one atom getting in-line with the rest along the applied force, suggesting an "atomic quantization" of the cross-section of the sample.

5 Metallic Clusters Deposited on Surfaces

The summation over ionic positions in the potential energy (3) can be restricted to certain space regions, for instance to a half-space corresponding to a semi-infinite solid with a free, plane surface at $x = 0$. In this case we may use the continuum approximation, *i.e.* we may replace the summation over ionic positions in (3) by an integration. We apply this procedure first to the self-consistent potential φ given by (2), and obtain

$$\varphi(x) = \frac{2\pi z^*}{q^2 a^3} \times \begin{cases} e^{-qx} & , \; x \geq 0 \\ \\ 2 - e^{qx} & , \; x < 0 \end{cases} \tag{5}$$

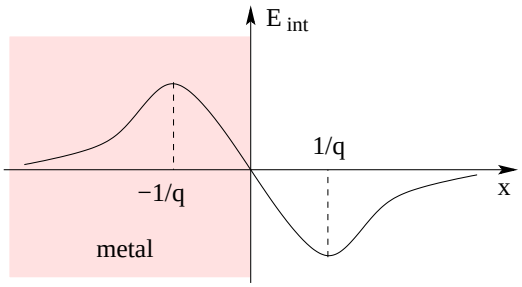

Figure 13: Interaction potential a metallic ion and a semi-infinite metal.

where z^* is the average effective charge and a denotes the average inter-ionic distance; as mentioned in Section 2 we may take $a \sim 2.73/q$ and $q \simeq 0.77 z^{*1/3}$, as for a metall. Comparing the self-consistent potential (5) with the bulk contribution $\varphi = 4\pi z^*/q^2a^3$ (obtained from (2) by integrating over the entire space), one can see that the surface brings its own contribution $\delta\varphi(x) = (2\pi z^*/q^2a^3)(x/\,|x|)e^{-q|x|}$ to the self-consistent potential, which, through the self-consistency relationship $n = (q^2/4\pi)\varphi$, entails a spill δn of the electrons over the surface and a charge double layer at the surface, as expected. The total charge distribution at the surface double layer is shown schematically in Fig. 12. The work function of the solid can be computed from (5), obtaining $\varphi = 4\pi z^*/q^2a^3$, as expected. The interaction energy $-(1/2)\int dx \cdot \delta\varphi\delta n$ associated with the electron double layer is $-\pi z^{*2}/2q^3a^6$ (per unit area), and it acts like an additional uncertainty in the quasi-particle energy, giving rise to boundary (finite-size) lifetime; it leads also to a weak relaxation of the ionic positions at the surface, which, however, is beyond the accuracy of the present computations. On the other hand, the potential energy (3) can be estimated for a semi-infinite metal in the continuum approximation, leading to

$$E_{pot} = -\frac{3}{4} q z^{*2} N + \frac{\pi z^{*2}}{2q^3a^6} A \ , \tag{6}$$

where the first term is the bulk contribution (N represents the number of ions in metal), while the second term is the surface contribution, A denoting the area of the cross-section; hence, one may derive the surface tension $\sigma = \pi z^{*2}/2q^3a^6$ of a metal; it agrees with the energy given above for the electron double layer.

Similarly, by using (3) and (4), we can estimate the interaction potential between a semi-infinite metal and a metallic ion with an effective charge z_0^* placed at distance x from the surface; we obtain

$$E_{pot} = E_s - \frac{3}{4} q z_0^{*2} - \frac{\pi z^* z_0^*}{qa^3} x e^{-q|x|} \ , \tag{7}$$

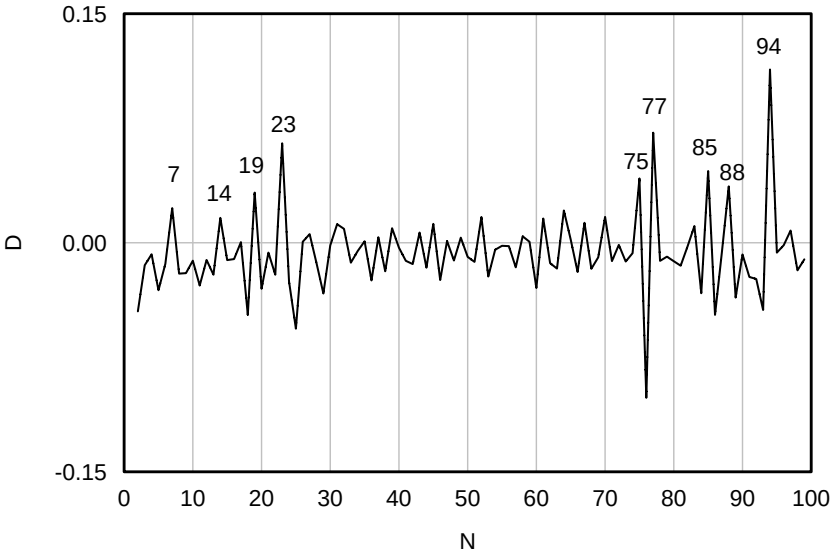

Figure 14: Ground-state mass spectrum of Fe-clusters deposited on Na-surface.

where E_s denotes the potential energy of the solid as given by (6); one can notice in (7) the self-energy of the added ion and the last term which represents the solid-ion interaction potential. This potential has an attractive tail above the surface and a repulsive barrier beneath, as shown in Fig. 12. The attractive part is responsible for forming up clusters added to the surface, while the interplay between the attractive and repulsive parts may determine the penetration of added atoms just beneath the surface, leading to diffusion and interfaces between a solid and a deposited cluster. It is worth noting that this interaction potential varies over a scale distance $\sim 1/q$, which is smaller than the average inter-ionic distance $a \sim 2.73/q$.

It is easy now, by making use of (7), to write down the potential energy of an ensemble of N metallic ions with effective charges z_i^* deposited on a metallic surface; it reads

$$E_{pot} = E_s - \frac{3}{4}q\sum_{i=1}^{N} z_i^{*2} + \frac{1}{2}\sum_{i\neq j=1}^{N} \Phi(R_{ij}) - \frac{\pi z^*}{qa^3}\sum_{i=1}^{N} z_i^* X_i e^{-q|X_i|} \quad , \qquad (8)$$

where the potentials $\Phi(R_{ij})$ are given by (4) and X_i denotes the x-coordinate of $\mathbf{R}_i$. It is worth noting that the screening wavevector q in (8) is the one of the solid, as the latter prevails upon the deposited cluster in the thermodynamic limit. In this respect, the deposited clusters differ from isolated clusters which have their own screening wavevector, as resulting from the

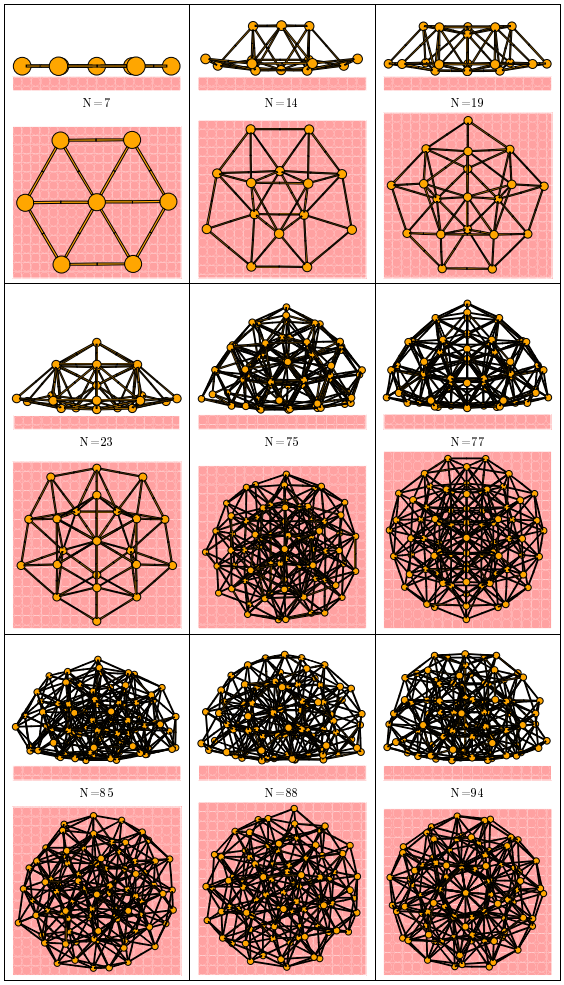

Figure 15: Magic Fe-clusters deposited on Na-surface, front view (upper rows) and top view (lower rows).

minimization of their quasi-classical energy. According to the theoretical approach presented in Section 2, the quasi-classical energy of the deposited cluster is $E_q = (27\pi^2/640)q^4 \sum_i z_i^* + E_{pot} - E_s$, and the binding energy is $E = E_q - (9/32)q^2 \sum_i z_i^*$. One can see here the separability of the general theoretical expression for the potential energy as given by (3) and (4) with respect to the ionic positions. We may also define an interaction energy from (8), between solid and a deposited cluster, by

$$E_{int} = -\frac{\pi z^*}{qa^3} \sum_{i=1}^{N} z_i^* X_i e^{-q|X_i|} \quad , \tag{9}$$

which may serve as a measure of the energy needed to separate the cluster off

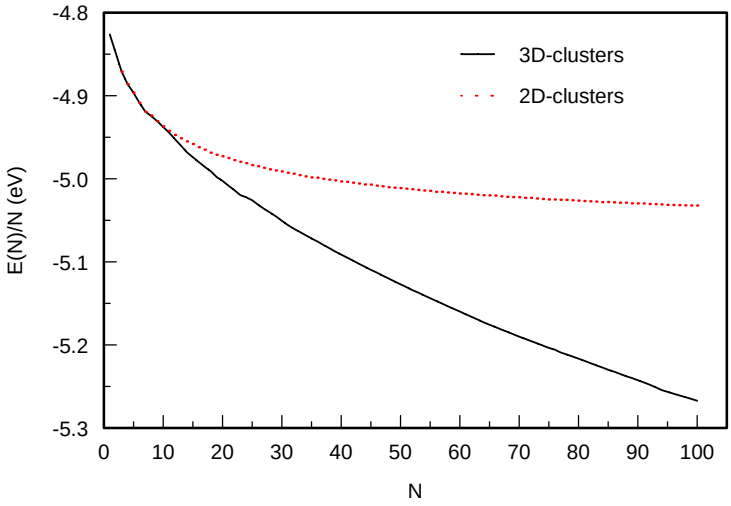

Figure 16: Ground-state energy per atom for Fe-clusters (3D, solid line) deposited on Na-surface *vs* cluster size, compared with monolayer cluster energy (2D, dashed line).

the surface (the difference in the cluster energy must be added, arising from its own screening wavevector corresponding to cluster relaxation). One can also check that the interaction energy (8) for the halves of a solid compensates exactly the surface energies of the two facets, as given by (6), as expected.

The main problem of depositing clusters on surface is the minimization of the potential energy given by (8) with respect to the ionic positions $\mathbf{R}_i$ (in fact, with respect to the reduced positions $q\mathbf{R}_i$). We follow the same procedure employed for isolated clusters, as described in Section 3, and illustrate the results here for Fe-clusters ($z^* = 0.57$) deposited on Na surface ($z^* = 0.44$). The ground-state mass spectrum for such clusters is shown in Fig. 14, up to $N = 100$. One can notice magic clusters deposited on surface like, for instance, those corresponding to $N = 7$, 14, 19, 23, 75, 77, 85, 88, 94...; they may acquire highly symmetric forms as those shown in Fig. 15. The principle of their packing seems to be the same "space economy"; for small values of N they arrange in rather regular polygons onto the surface, but with increasing N they start to construct up vertically, by adding successively multiple terraces, more or less regular; the overall constructions exhibit often a wonderfully intricate geometry, as one can see in Fig. 15 for $N = 23, 77, 94$, suggesting hats, theaters, stadia, domes, etc. In general, there is a competition between growing up vertically and laying down horizontally along the surface. We obtain monolayers (2D clusters) as ground-states for $N \leq 7$ and as isomers for $N > 7$, as shown in Fig. 16, where their binding energy

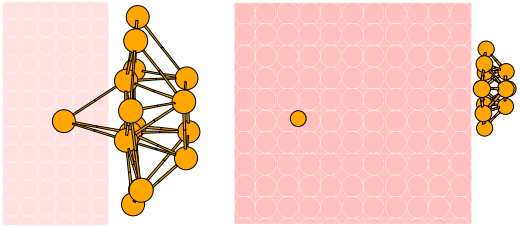

(a) (b)

Figure 17: (a) A deposited cluster with one ion beneath the surface. (b) An ion diffused into solid from a deposited cluster.

is compared with the ground-state energy of deposited clusters (3D). We obtain also isomers, as expected, some of them with strange constructions close to unstability (*i.e.* with high energies). There are many curiosities in constructing such deposited clusters, as for instance, the rather structureless island between $N = 23$ and $N = 75$ in Fig. 14, which is intriguing. Some of the constructions obtained here theoretically can be found in experimental works.[16] In this connection it is worth noting that the continuum approximation employed here is, in fact, unnecessary, though useful; it affects the proximity properties between clusters and surface, and, of course, the problem of the "lattice constants" matching.

Finally, it is worth presenting a very interesting situation shown in Fig. 17a, where one added ion has penetrated beneath the surface, the rest having remained at the surface and formed there a deposited cluster. The ion goes through the potential barrier shown in Fig. 13, and is kept in equilibrium by the interplay between the metal attraction and the surface-cluster attraction, which act in opposite directions. Such a cluster exhibiting an incipient interface with the solid is always an isomer, *i.e.* its energy is higher than the ground-state energy of a cluster of the same size deposited on surface. There appears also the possibility of a penetrating ion to escape into the solid, as shown in Fig. 17b, where the position of the ion in solid is practically undefined, *i.e.* this ion is free; it has diffused into the solid. A more sizeable number of atoms may penetrate beneath the surface, as shown in the first two pictures in Fig. 18 for a 50-atoms cluster, or for a 100-atoms cluster which developed a well-defined incipient interface with the solid (last picture in Fig. 18). These formations are incipient quantum dots of a very small size. Such results are encouraging for applying the present theoretical approach to more complex situations, in particular to nanostructures exhibiting interfaces, or other geometric and dynamic particularities.

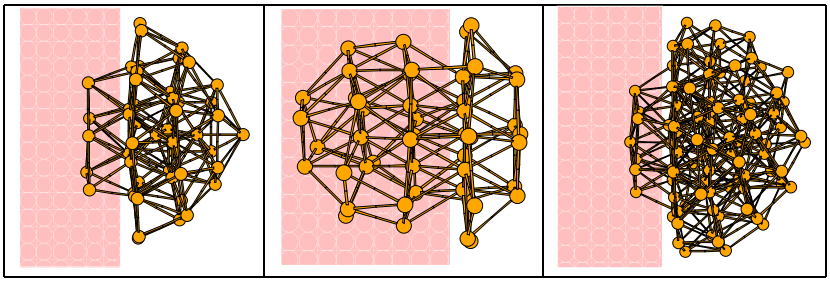

Figure 18: A 50-atoms cluster diffusing beneath a solid surface (first two pictures), and a 100-atoms cluster developing an incipient interface with a solid (last picture in the row).

6 Other Effective Potentials

The self-consistent Hartree field (2) was obtained for point-like ionic charge distributions. Preserving the quasi-classical self-consistency

$$n = (q^2/4\pi)\varphi \ , \tag{10}$$

we can give a formal solution for the Hartree field φ for a general background charge distribution ρ by solving the linear equation

$$\Delta\varphi(\mathbf{r}) = -4\pi\rho(\mathbf{r}) + q^2\varphi(\mathbf{r}) \ ; \tag{11}$$

which is obtained from Poisson equation by making use of (10); the solution of this equation is[3]

$$\varphi(\mathbf{r}) = \int d\mathbf{r}' \frac{\rho(\mathbf{r}')}{|\mathbf{r}-\mathbf{r}'|} e^{-q|\mathbf{r}-\mathbf{r}'|} \ . \tag{12}$$

For the point-like charge distribution (1) the self-consistent field (2) is re-obtained but now we can write the general solution

$$\varphi(r) = \sum_{i=1}^{N} \int d\mathbf{r}' \frac{\rho_i(\mathbf{r}'-\mathbf{R}_i)}{|\mathbf{r}-\mathbf{r}'|} e^{-q|\mathbf{r}-\mathbf{r}'|} \ , \tag{13}$$

[3]In general, we can write the solution as $\varphi(\mathbf{r}) = \int d\mathbf{r} G(\mathbf{r},\mathbf{r}')\rho(\mathbf{r}')$, where $G(\mathbf{r},\mathbf{r}')$ is the Green function (or the resolvent) of the homogeneous equation

$$(\Delta - q^2)G(\mathbf{r},\mathbf{r}') = -4\pi\delta(\mathbf{r}-\mathbf{r}') \ .$$

The solution of this equation, $G(\mathbf{r},\mathbf{r}') = \exp(-q|\mathbf{r}-\mathbf{r}'|)/|\mathbf{r}-\mathbf{r}'|$ leads to the above expression for the self-consistent field φ.

for a nano-aggregate with N atoms with the core charge distributions $\rho_i(\mathbf{r})$ and the atomic positions $\mathbf{R}_i$ ($\rho(\mathbf{r}) = \sum_{i=1}^{N} \rho_i(\mathbf{r} - \mathbf{R}_i)$). Starting from this potential and the corresponding electron density given by (10) we can follow the same steps as in Section 2 and derive the kinetic energy, the potential energy, the quasi-classical energy and the exchange correction; as before we will identify a general expression for the effective inter-ionic potential.

The potential energy is given by

$$E_{pot} = E_c - \frac{1}{2} \int d\mathbf{r} \cdot n \left(\varphi + \varphi_c \right) \tag{14}$$

where

$$E_c = \frac{1}{2} \sum_{i \neq j} \int d\mathbf{r}_1 d\mathbf{r}_2 \frac{\rho_i(\mathbf{r}_1 - \mathbf{R}_i)\rho_j(\mathbf{r}_2 - \mathbf{R}_j)}{|\mathbf{r}_1 - \mathbf{r}_2|} \tag{15}$$

is the potential energy of the atomic cores and

$$\varphi_c(\mathbf{r}) = \sum_{i=1}^{N} \int d\mathbf{r}' \frac{\rho_i(\mathbf{r}' - \mathbf{R}_i)}{|\mathbf{r} - \mathbf{r}'|} \tag{16}$$

is the ionic-core contribution to the self-consistent potential. Using (10), after performing the integration over $\mathbf{r}$, the intervening integrals being of two-center type, the potential energy (14) reads

$$\begin{gathered} E_{pot} = -\tfrac{1}{4} q \textstyle\sum_i \epsilon_i - \\ -\tfrac{1}{4} q \textstyle\sum_{i \neq j} \int d\mathbf{r}_1 d\mathbf{r}_2 \rho_i(\mathbf{r}_1 - \mathbf{R}_i)\rho_j(\mathbf{r}_2 - \mathbf{R}_j) v(q\,|\mathbf{r}_1 - \mathbf{r}_2|) \ , \end{gathered} \tag{17}$$

where $v(x) = (1 - 2/x)e^{-x}$ and ϵ_i plays the role of an ionic "self-energy" given by

$$\epsilon_i = \int d\mathbf{r}_1 d\mathbf{r}_2 \rho_i(\mathbf{r}_1)\rho_i(\mathbf{r}_2) \left[e^{-q|\mathbf{r}_1 - \mathbf{r}_2|} + 2 \frac{1 - e^{-q|\mathbf{r}_1 - \mathbf{r}_2|}}{q\,|\mathbf{r}_1 - \mathbf{r}_2|} \right] \ . \tag{18}$$

Because, usually $\rho_i(\mathbf{r})$ is exponentially vanishing at large distance, the main contribution to the ionic self-energy is obtained for $|\mathbf{r}_1 - \mathbf{r}_2| \ll 1$, therefore we have

$$\epsilon_i \simeq 3 \left[\int d\mathbf{r} \rho_i(\mathbf{r}) \right]^2 = 3 z_i^{*2} \ , \tag{19}$$

where $z_i^* = \int d\mathbf{r} \rho_i(\mathbf{r})$ is the effective valence charge of the i-th atom. For homo-atomic clusters we obtain the total ionic self-energy $3Nz^*$, where $z^* = z_i^*$ =constant.

The last term in the potential energy (17) corresponds to effective inter-ionic potentials

$$\Phi_{ij}(\mathbf{R}_i,\mathbf{R}_j) = -\tfrac{1}{2}q\int d\mathbf{r}_1 d\mathbf{r}_2 \rho_i(\mathbf{r}_1-\mathbf{R}_i)\rho_j(\mathbf{r}_2-\mathbf{R}_j)\times \\ \times\left(1-\tfrac{2}{q|\mathbf{r}_1-\mathbf{r}_2|}\right)e^{-q|\mathbf{r}_1-\mathbf{r}_2|} \quad . \tag{20}$$

which depends on the atomic species and positions.

For homo-atomic clusters (single-component clusters) the core charge distribution is the same for all atoms, $\rho_i(\mathbf{r}) = \rho_j(\mathbf{r}) \doteq \rho_c(\mathbf{r})$ and the effective inter-atomic potential depends only on the atomic positions. Obviously, for atoms with spherically symmetric core charge distribution the above potential depends only on the inter-atomic distance. For example, in the point-like ion approximation $\rho_c(\mathbf{r}) = z^*\delta(\mathbf{r})$, we re-obtain the potential given by (4), as expected. It is worth mentioning here that long time ago a similar potential has been suggested on semi-empirical grounds, with some success, for the H_2 molecule.[20]

We can apply these expressions to various situations ranging from spatially extended ions to interactions between nanostructures and macroscopic solids; all we have to known is the form of the positive charge distributions. Before giving a few interesting examples we would like to explain the multi-particle character of these effective interactions. For a constant screening wavevector q, these potentials describe genuine two-particle interactions. However, this picture is essentially altered if we follow the quasi-classical prescriptions used in deriving the above effective potentials. In the quasi-classical description[3] q is determined by minimizing the quasi-classical energy; therefore it has a slow dependence on the atomic positions. The quasi-classical energy is obtained by adding to the potential energy (17) the kinetic energy contributions:

$$E_{kin} = \frac{27\pi^2}{640}q^4\sum_{i=1}^{N}\int d\mathbf{r}\rho_i(\mathbf{r}) = \frac{27\pi^2}{640}q^4\sum_{i=1}^{N} z_i^* \quad , \tag{21}$$

which has the same form as for point-like ions. We obtain the quasi-classical functional

$$E_q = E_{kin} - \frac{1}{4}q\sum_i \epsilon_i + \frac{1}{2}\sum_{i\neq j}\Phi_{ij} \quad , \tag{22}$$

where ϵ_i and Φ_{ij} have been introduced above. In principle, the ionic self-energy has a slow q-dependence. We have shown that, for atoms with rapidly vanishing core charge distribution, the point-like ion solution $\epsilon_i = 3z^*$ is a

good approximation. Therefore we will neglect this q-dependence. It is expected that for very large atoms this dependence may become important.

The parameter q is obtained by the minimum condition

$$\frac{\partial E_q}{\partial q} = 0 \ . \tag{23}$$

In this way, q is a global parameter which depend on all atomic positions $\mathbf{R}_i$. In this respect the above potentials have a multi-particle (N-particle) character. Equation (23) gives

$$\frac{27\pi^2}{160}\overline{z}q^3 - \frac{1}{4}\epsilon - \frac{1}{4N}\sum_{i\neq j}\int d\mathbf{r}_1 d\mathbf{r}_2 \rho_i(\mathbf{r}_1)\rho_j(\mathbf{r}_2) g\left(q\left|\mathbf{r}_1 - \mathbf{r}_2 + \mathbf{R}_i - \mathbf{R}_j\right|\right) \ , \tag{24}$$

where $g(x) = (3-x)\exp(-x)$, $\bar{z} = \frac{1}{N}\sum_i z_i^*$ is the mean valence charge and $\epsilon = \frac{1}{N}\sum_i \epsilon_i$ is the mean ionic self-energy. The first two terms are dominant, giving the asymptotic solution ($|\mathbf{R}_i - \mathbf{R}_j| \to \infty$)

$$q_0 = \frac{2}{3\pi}\left(5\pi\frac{\epsilon}{\bar{z}}\right)^{1/3} \ , \tag{25}$$

which leads to the bare two-particle interaction Φ_{ij}^0.

Equation (24) can be written as

$$q^3 - q_0^3 = q_0^3 \frac{1}{\epsilon N}\sum_{i\neq j} G_{ij} \ , \tag{26}$$

where

$$G_{ij} = \int d\mathbf{r}_1 d\mathbf{r}_2 \rho_i(\mathbf{r}_1)\rho_j(\mathbf{r}_2) g\left(q_0\left|\mathbf{r}_1 - \mathbf{r}_2 + \mathbf{R}_i - \mathbf{R}_j\right|\right) \ . \tag{27}$$

Treating the *r.h.s.* of the above equation (the interaction part) as a small perturbation which lead to small variations in q around the free value q_0, we obtain in the first order

$$\begin{aligned} q &= q_0\left(1 + \frac{1}{\epsilon N}\sum_{i\neq j} G_{ij}\right)^{1/3} \\ &\cong q_0 + \frac{q_0}{3\epsilon N}\sum_{i\neq j} G_{ij} \ . \end{aligned} \tag{28}$$

The interaction energy is

$$V = \frac{1}{2}\sum_{i\neq j}\Phi_{ij} \cong \frac{1}{2}\sum_{i,j}\Phi^0_{i,j} + \frac{1}{2}\sum_{i,j}\left(\frac{\partial\Phi_{ij}}{\partial q}\right)_{q_0}\delta q \ . \tag{29}$$

The first term is a superposition of two-particle bare interaction potentials; the second term will give corrections to this two-body potential (the dressing phenomenon) and a three- and a four-body interaction. Higher order solutions for q will continue to dress up the two-body interaction, and in addition will give highest order many-body potentials:

$$V = \underbrace{\frac{1}{2}\sum_{i,j}\Phi^0_{ij} + ...}_{\text{two-particle+dressing}} + \underbrace{v_3 + ...}_{\text{three-particle}} + \underbrace{v_4 + ...}_{\text{four-particle}} + ... \tag{30}$$

The first order solution give the dressing correction to the bare two-body interaction

$$\delta v_2 = -\frac{q_0}{6\epsilon N}\sum_{i,j} G_{ij} \ \ , \tag{31}$$

and three and four-body interaction potentials

$$v_3 = -\frac{q_0}{3\epsilon N}\sum_{i\neq j\neq k} G_{ij}G_{jk} \ , \ v_4 = -\frac{q_0}{12\epsilon N}\sum_{i\neq j\neq k\neq l} G_{ij}G_{kl} \ . \tag{32}$$

It is worth noting that this expansion is valid at large distances where the bare two-body interaction is dominant. When the inter-atomic distances become close to the binding distances, the higher order multi-particle potentials become also important. In the vicinity of the equilibrium positions all the terms are important and must be taken into account. This expansion is used only to illustrate the multi-particle character and the medium dependence of these potentials. In order to get the equilibrium positions we must minimize the quasi-classical energy with respect to the atomic positions $\mathbf{R}_i$ and the screening wavevector q. In other words, we must solve first equation (24) and then include the expression thus obtained for q in E_q; we obtain in this way an expression for the cluster energy dependent only on the atomic positions $\mathbf{R}_i$ which can be minimized to get the equilibrium positions.

A major simplification occurs if the core-charge distribution is a n-th order homogeneous function,

$$\rho(\lambda\mathbf{r}) = \lambda^n\rho(\mathbf{r}) \ \ . \tag{33}$$

Since $\int d\mathbf{r}\rho_i(\mathbf{r}) = z_i^*$, the only possible situation is $n = -3$. In this case the quasi-classical energy functional (22) can be written as

$$\begin{aligned} E_q = \tfrac{27\pi^2}{640} q^4 \textstyle\sum_{i=1}^N z_i^* - \tfrac{1}{4} q \textstyle\sum_i \epsilon_i - \\ -\tfrac{1}{4} q \textstyle\sum_{i\neq j} \int d\mathbf{r}_1 d\mathbf{r}_2 \rho_i(\mathbf{r}_1)\rho_j(\mathbf{r}_2) v(|\mathbf{r}_1 - \mathbf{r}_2 + \mathbf{X}_i - \mathbf{X}_j|) \ , \end{aligned} \tag{34}$$

where we have introduced the dimensionless variables $\mathbf{X}_i = q\mathbf{R}_i$ and ϵ_i is not q-dependent anymore; it is given by

$$\epsilon_i = \int d\mathbf{r}_1 d\mathbf{r}_2 \rho_i(\mathbf{r}_1)\rho_i(\mathbf{r}_2) \left[e^{-|\mathbf{r}_1 - \mathbf{r}_2|} + 2\frac{1 - e^{-|\mathbf{r}_1 - \mathbf{r}_2|}}{|\mathbf{r}_1 - \mathbf{r}_2|} \right] \ . \tag{35}$$

In this case the two minimization steps can be inverted. The equilibrium geometric forms of nano-aggregates are obtained by minimizing the reduced interaction term in equation (34),

$$E_{int} = -\sum_{i\neq j} \int d\mathbf{r}_1 d\mathbf{r}_2 \rho_i(\mathbf{r}_1)\rho_j(\mathbf{r}_2) v(|\mathbf{r}_1 - \mathbf{r}_2 + \mathbf{X}_i - \mathbf{X}_j|) \ , \tag{36}$$

with respect to the dimensionless variables $\mathbf{X}_i$. The resulting value for this interaction energy is used in the second step: the minimization of the quasi-classical energy with respect to the screening wavevector q. The equilibrium value is given by

$$q = q_0 \left(1 + \frac{1}{\epsilon N} |E_i| \right)^{1/3} \ , \tag{37}$$

where q_0 and ϵ have been introduced above. Thereafter, the atomic positions are derived from $\mathbf{R}_i = \mathbf{X}_i/q$.

Though the condition (33) is fulfilled in the point-like ion approximation, more realistic core charge distributions do not have this property. For example, for the hard core ionic charge distribution, $\rho(r) = \rho_o \theta(a - r)$, where a is the radius of the ionic core, with constant charge density $\rho_0 = z^* 3/4\pi a^3$, we obtain the effective inter-atomic potential

$$\Phi(|\mathbf{R}_i - \mathbf{R}_j|) = -\frac{1}{2} q z^{*2} \alpha_1^2 \left(1 - \beta_1 \frac{2}{q\,|\mathbf{R}_i - \mathbf{R}_j|} \right) e^{-q|\mathbf{R}_i - \mathbf{R}_j|} \ , \tag{38}$$

for $|\mathbf{R}_i - \mathbf{R}_j| > 2a$, where

$$\begin{aligned} \alpha_1 &= 3\tfrac{qa\cosh qa - \sinh qa}{(qa)^3} \ , \\ \beta_1 &= \tfrac{2qa\cosh qa - (2+q^2a^2)\sinh qa}{\sinh qa - qa\cosh qa} \ . \end{aligned} \tag{39}$$

We can see that in the limit $a \to 0$ we have $\alpha_1 \to 1$, $\beta_1 \to 1$, re-obtaining, as expected, the effective-potential in the point-like ion approximation. Except for the explicit dependence on q, as discussed above for non-homogeneous charge distributions, there are no major differences compared to the point-like ion potential. The shape of the potential is the same. Also, for reasonable values for a and q we get quantitatively the same results. For example, for $a = 1$ and $q = 0.5$ we get $\alpha_1 = 1.02$ and $\beta_1 = 1.05$.

For a more realistic core charge distribution $\rho(\mathbf{r}) = Z\delta(\mathbf{r}) - \rho_0\theta(a - r)$, where the first term correspond to the nucleus charge Z and the last term correspond to the core electrons with constant $\rho_0 = 3(Z - z^*)/4\pi a^3$ density inside of a sphere of radius a (the ion radius) centered around the nucleus, we get the same form for the effective inter-atomic potential

$$\Phi(|\mathbf{R}_i - \mathbf{R}_j|) = -\frac{1}{2}qz^{*2}\alpha_2^2\left(1 - \beta_2\frac{2}{q\,|\mathbf{R}_i - \mathbf{R}_j|}\right)e^{-q|\mathbf{R}_i - \mathbf{R}_j|} \ , \qquad (40)$$

with

$$\begin{aligned} \alpha_2 &= \alpha_1 + \tfrac{Z}{z^*}(\alpha_1 - 1) \ , \\ \beta_2 &= \beta_1\alpha_1^2 + \tfrac{Z^2}{z^{*2}}(1 + \alpha_1^2\beta_1 - 2\gamma\alpha_1) + 2\alpha_1\tfrac{Z}{z^*}(\gamma - \alpha_1\beta_1) \ , \end{aligned} \qquad (41)$$

where $\alpha_1$and β_2 are given by equations (39) and

$$\gamma = \frac{1}{2}\frac{qa\cosh qa - (1 + q^2a^2)\sinh qa}{\sinh qa - qa\cosh qa} \ . \qquad (42)$$

Again, the point-like ion result is re-obtained in the limit $a \to 0$.

The general expression for the self-consistent field (12) can be used in deriving the self-consistent potential of a semi-infinite solid. Writing the background charge density as $\rho(\mathbf{r}) = \rho_0 \cdot \theta(-x)$ we obtain from equation (12) the self-consistent potential[17]

$$\varphi(\mathbf{r}) = \frac{2\pi\rho_0}{q^2} \times \begin{cases} e^{-qx} & , \ x \geq 0 \\ 2 - e^{qx} & , \ x < 0 \end{cases} \qquad (43)$$

and the electron density

$$n(\mathbf{r}) = \rho_0 \times \begin{cases} \frac{1}{2}e^{-qx} & , \ x \geq 0 \\ 1 - \frac{1}{2}e^{qx} & , \ x < 0 \end{cases} \qquad (44)$$

which is the well known Smoluchowski density,[18] used often with good results as a trial electron density function for metallic surfaces (see, for instance,

Ref. [19]). The present theoretical approach provides, probably for the first time, the derivation for this relation. In Section 5 we have obtained these expressions (see eq. (5)) by taking the continuum limit in equation (2).[17] These two methods are equivalent.

Let us consider another example. For an atomic nano-slab of thickness L with a free surface placed at $x = 0$ and the other one at $x = -L$ we obtain the self-consistent potential

$$\varphi(x) = \frac{2\pi\rho_0}{q^2} \times \begin{cases} e^{-q|x|} - e^{-q|x+L|} & , \ x \geq 0 \text{ or } x \leq L \\ 2 - e^{qx} - e^{-q(x+L)} & , \ -L \leq x < 0 \end{cases} , \qquad (45)$$

for a constant background charge density ρ_0. For $L \to \infty$, as for a semi-infinite solid, we re-obtain equation (43); for $L \to 0$, as for a thin infinite plate with a surface charge density $\rho L \to \sigma$, we obtain an exponentially decreasing potential, $\varphi = 2\pi\sigma \exp(-q|x|)/q$. Using equation (20) we can calculate the interaction potential in the jellium approximation between two such nano-structures. We get the interaction potential per unit area

$$\Phi(d) = -\frac{\pi\sigma^2}{q} e^{-qd}(qd - 1) \ , \qquad (46)$$

for two parallel infinite plates with the positive surface charge distribution σ placed at a distance d. A finite numbers of such plates forms equilibrium structures with one dimensional behaviors. The electron distributions for this type of structures has been recently investigated using an numerical approach to the Thomas-Fermi model.[21] We can obtain these densities analytically.

A very interesting application is the interaction between two semi-infinite solids. Various electronic structure calculations have given support for the existence of an universal scaling of binding energies;[19, 22] it appears that these energies divided by their minimum values are well represented by the Rydberg function

$$E^*(\widetilde{d}) = -(1 + \beta\widetilde{d})e^{-\beta\widetilde{d}} \ , \qquad (47)$$

where $\widetilde{d} = (d - d_m)/l$ with d_m being the equilibrium distance and l a scale length whose values could be given by the Thomas-Fermi screening length.[19]

We obtain, from equation (20), the interaction per unit area

$$\Phi(d) = -\frac{\pi\rho_0^2}{q^3}(1 + q|d|)e^{-q|d|} \qquad (48)$$

for two solids at distance d with background charge density ρ_0. This potential has a minimum for $d_m = 0$, that is for solids in contact; it is worth nothing that in the continuum approximation from which this potential is derived the inter atomic distances, which represent a measure for d_m, has been taken as being infinitesimally small. Moreover, the screening wave vector q depends on a variationally Thomas-Fermi wavevector through, $q^2 = 8\bar{k}_F/3\pi$;[3] introducing a (variationally) Thomas-Fermi screening length through $1/\bar{\lambda}_{TF} = (4\bar{k}_F/\pi)^{1/2}$, we can write $q = (2/3)^{1/2}/\bar{\lambda}_{TF}$. As above, dividing by the minimum absolute value $\pi\rho_0^2/q^3$, we can define

$$\Phi^*(\tilde{d}) = -(1 + \beta|\tilde{d}|)e^{-\beta|\tilde{d}|} \tag{49}$$

where $\beta = (2/3)^{1/2}$ and $\tilde{d} = d/\bar{\lambda}_{TF}$, consistent with our jellium model. We can see that for $\tilde{d} \geq 0$ (or $d \geq d_m$) we have obtained the form (47) suggested in Ref. [22]. Moreover, our value for $\beta(= (2/3)^{1/2})$ is close to the value $\beta = 0.9$ which provided the best fit in Ref. [22]. We must note that we can directly identify a screening length as $\lambda_{TF} = 1/q$; in this case $\beta = 1$ also close to the 0.9 best fit value. Moreover, if we take a mean value between the two methods of defining λ_{TF} we get $\beta \simeq 0.908$ which is astonishingly close to the fit value.

7 Concluding Remarks

The theoretical approach presented here deals with matter aggregation at the atomic level. It is based on the quasi-classical solution to Hartree-Fock equations describing a neutral ensemble of Coulomb interacting ions and valence electrons. The main ingredient of the theory is an inter-ionic effective (pseudo-) potential, of the type given by (4) for point-like effective ionic charges. The model has been applied to several species of metallic ions, leading to formation of homo-atomic clusters, either isolated or deposited on surfaces, as well as to some peculiar nanostructures, both with geometric and dynamic constraints. It provides quantitative results for geometric forms, ionic positions, inter-ionic distances, binding energies, both of ground-states and isomers, clusters stability and vibration spectra. Magic clusters and magic numbers have been obtained for ground-states, giving an insight into the geometric patterns of cluster aggregation. At this level, the theoretical approach has a first-step approximation character, the full treatment requiring the so-called quantum corrections. These provide single-particle properties, like electron energy levels, ionization potentials, chemical affini-

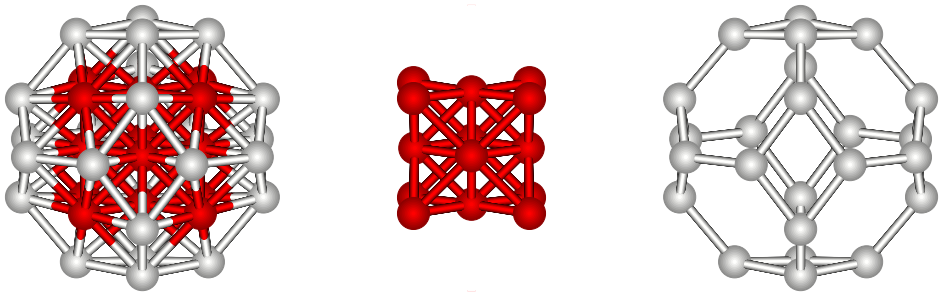

Figure 19: The magic cluster $A_{14}B_{28}$ (*left*) with a *fcc* $A-$core (*center*) and an outside $B-$shell (*right*).

ties, as well as response to external fields, transport and various spectroscopical properties included. The quantum corrections set also the ground for treating the clusters magnetism. The latter originates mainly in the electron ferromagnetism, as caused by the exchange interaction, and the ionic paramagnetism; both are to be treated in the particular context of a single-domain (or a few domains) magnetism, and a fractional occupancy of the electron levels, as required by the effective charge parameters. Both localized and itinerant magnetic moments are specific to clusters magnetism, with particular properties, like high, inhomogeneous magnetization, super-paramagnetism, etc. In addition, the model must be further refined by taking into account the spatial structure of the ionic charge distribution, in particular its angular dependence in oriented chemical bonds. This would considerably enlarge the applicability of the theory to large classes of chemical species.

Another interesting application is cohesion in hetero-atomic structures. A study of binary metallic clusters consisting of a large variety of atoms types is currently underway. We find that increasing the discrepancy between the two types of atoms (increasing the ratio between theirs effective valence charges) leads to a gradually decrease of the homo-atomic magic (total) numbers and the appearance of magic pairs like (6,32), (10,22), (13,20), (14,24) or (26,12). The equilibrium structures are in general core-shell clusters with the atoms of greater z^* in the center. Although the icosahedral symmetry is still dominant, the double magic clusters have sometime cubic symmetries like, for example, the $A_{14}B_{22}$ cluster presented in Fig. 19, magic (or double magic) for $1.4 \leq z_A^*/z_B^* \leq 2$; its core is a face centered cube and the outside shell is a truncated octahedron. The *bcc* symmetry has been obtained for the A_9B_6 cluster; in the range $1.4 \leq z_A^*/z_B^* \leq 2.3$ the A atoms forms a single *bcc* cell while the B atoms find equilibrium positions in the vicinity of the nearest neighbour centers.

Acknowledgments

The authors are indebted to the members of the Laboratory of Theoretical Physics at Magurele-Bucharest for helpful discussions and many illuminating insights at various stages of this work.

References

[1] M. Apostol, J. Theor. Phys. **55** 82 (2000); *ibid*, **60** 125 (2000).

[2] See, for instance, J. A. Pople, Revs. Mod. Phys. **71** 1267 (1998) for a review.

[3] L. C. Cune and M. Apostol, Phys. Lett. **A273** 117 (2000); see also L. C. Cune and M. Apostol, *Metallic Binding*, **apoma**, MB (2000).

[4] See, for instance, W. Kohn, Revs. Mod. Phys. **71** 1253 (1998).

[5] J. C. Slater, *Quantum Theory of Atomic Structure*, McGraw-Hill, NY (1960).

[6] E. Wigner and F. Seitz, Phys. Rev. **43** 804 (1934); *ibid*, **46** 509 (1934); E. Wigner, Phys. Rev. **46** 1002 (1934); Trans. Faraday Soc. **34** 678 (1938).

[7] J. C. Slater, *The Calculations of Molecular Orbitals*, Wiley, NY (1979).

[8] See in this context the "no-binding" theorem in E. Lieb and B. Simon, Adv. Math. **23** 22 (1977), and L. Spruch, Revs. Mod. Phys. **63** 151 (1991).

[9] J. Schwinger, Phys. Rev. **A24** 2353 (1981); see also *ibid*, **A22** 1827 (1980).

[10] Second reference cited under Ref. 3.

[11] See, for instance, J. P. K. Doye and D. J. Wales, J. Chem. Soc. Faraday Trans. **93** 4233 (1997); W. A. de Heer, Revs. Mod. Phys. **65** 611 (1993), M. Brack, Revs. Mod. Phys. **65** 677 (1993) and references therein; D. Rayane, P. Melinon, B. Tribollet, B. Chabaud, A. Hoareau and M. Broyer, J. Chem. Phys. **91** 3100 (1990).

[12] B. I. Dunlap, Phys.Rev. **A41** 5691 (1990); M. Castro and D. R. Salahub, Phys. Rev. **B47** 10 955 (1993); O. B. Christensen and M. L. Cohen, *ibid*, **B47** 13 643 (1993); Q. Wang, Q. Sun, M. Sakurai, J. Z. Yu, B. L. Gu, K. Sumiyama and Y. Kawazoe, Phys. Rev. **B59** 12 672 (1999).

[13] V. Bonacic-Koutecki, P. Fantucci and J. Koutecki, Phys. Rev. **B37** 4369 (1988); J. Chem. Phys. **93** 3802 (1990); Chem. Rev. **91** 1035 (1991); P. Ballone, W. Andreoni, R. Car and M. Parinello, Europhys. Lett. **8** 73 (1989); W. Andreoni, Z. Phys. **D19** 31 (1991); U. Rothlisberger and W. Andreoni, J. Chem. Phys. **94** 8129 (1991); W. A. de Heer, W. D. Knight, M. Y. Chou and M. L. Cohen, in H. Ehrenreich and D. Turnbull (eds), *Solid State Physics*, Academic, NY (1987), vol. **40**, p. 93; C. Brechignac, P. Cahuzac, F. Carlier, M. de Frutos and J. Leygnier, Chem. Phys. Lett. **186** 28 (1992); C. Brechignac, P. Cahuzac, M. de Frutos, J. P. Roux and K. H. Bowen, in P. Jena et al (eds), *Physics and Chemistry of Finite Systems: From Clusters to Crystals*, Kluwer, Academic, Dordercht (1992), vol. **1**, p. 369.

[14] F. Huisken , B. Kohn, R. Alexandrescu and I. Morjan, J. Chem. Phys. **113** 6579 (2000).

[15] L. C. Cune and M. Apostol, Chem. Phys. Lett. **344** 287 (2001).

[16] See, for instance, K.-H. Meiwes-Broer (ed), *Metal Clusters at Surfaces: Structure, Quantum Properties, Physical Chemistry (Cluster Physics)*, Springer (2000).

[17] L. C. Cune and M. Apostol, in *Low-Dimensional Systems: Theory, Preparation, and Some Applications*, eds. Luis M. Liz-Marzan et al., Kluwer, Academic (2003), p.1.

[18] R. Smoluchowski, Phys. Rev. **60** 661 (1941).

[19] A. Kiejna and K.F. Wojciechowski , *Metal Surface Electron Physics*, Pergamon (1996).

[20] A. A Frost and B. Musulin, J. Chem. Phys. **22** 1077 (1954).

[21] R. J. Komlos and A Rabinovitch, Phys. Lett. **A372** 6670 (2008).

[22] J. H. Rose, J. Ferrante and J. R. Smith, Phys. Rev. Lett. **47** 675 (1981).